

Integrity-constrained Factor Graph Optimization for GNSS Positioning

Xiao Xia

Department of Aeronautical and
Aviation Engineering
The Hong Kong Polytechnic University
Hong Kong, China
xxiao.xia@connect.polyu.hk

Li-Ta Hsu*

Department of Aeronautical and
Aviation Engineering
The Hong Kong Polytechnic University
Hong Kong, China
lt.hsu@polyu.edu.hk

Weisong Wen

Department of Aeronautical and
Aviation Engineering
The Hong Kong Polytechnic University
Hong Kong, China
welson.wen@polyu.edu.hk

Abstract— The concept of global navigation satellite system (GNSS) integrity refers to the measure of trust of the GNSS positioning solution, which is vital for safety-critical applications such as aviation and autonomous driving. While integrity monitoring was firstly introduced and widely applied in the GNSS aviation field, it is not suitable for GNSS positioning in urban scenarios due to unique circumstances such as limited satellite visibility, strong multipath and non-line-of-sight (NLOS) effects. For example, the direct exclusion of the GNSS multipath and NLOS would significantly degrade the geometry constraints, thus leading to highly conservative integrity monitoring (IM). As a result, the limited GNSS measurement redundancy and the inaccurate measurement uncertainty modeling in urban canyons will severely degrade the performance of both the GNSS positioning and integrity monitoring. To alleviate these issues, this paper proposed an integrity-constrained factor graph optimization (FGO) for GNSS positioning with the help of switchable constraints. Compared to the conventional GNSS IM methods which consider measurements in single epoch or two successive epochs, the proposed method improves the measurement redundancy by the factor graph structure. Meanwhile, the switch variable, which is introduced by switchable constraints and connected with each pseudorange measurement, can not only estimate the measurement uncertainties, but also satisfying the Chi-square testing of the conventional fault detection and exclusion (FDE) while maintaining satellite geometry. In particular, the calculated protection levels consider the effect of switch variables, hence bound the position error more accurately. The performance of this proposed method is evaluated on open-sky dataset with manually injected biases with gaussian random noise.

Keywords— *integrity monitoring, factor graph optimization, switch variables, fault detection and exclusion, urban positioning*

I. INTRODUCTION

Global Navigation Satellite System (GNSS) has obtained wide applications in diverse areas such as aviation and autonomous vehicles due to its ability to continuously provide high-accurate global position, velocity, and timing information throughout the day [1]. While the early stage of positioning applications focuses mainly on the accuracy, integrity concepts are vital for safety-critical applications [2]. To be specific, GNSS integrity refers to the measure of trust of the positioning solution supplied by the whole navigation system. Integrity monitoring provides the system with the ability to timely warn the users of the unavailable status, whereas incorrect integrity monitoring could result in devastating consequences [1]. By exploiting the redundancy of the available observations, integrity monitoring

(IM) can also be performed at the user level, which includes both Fault Detection and Exclusion (FDE) and Protection Level (PL) calculations [3].

The concept of Receiver Autonomous Integrity Monitoring (RAIM) [4] was firstly introduced in the aviation field. Particularly, RAIM provides the ability to monitor the system integrity and alert faulty in time by exploiting redundant measurements to conduct the consistency check of an overdetermined solution. However, it only considers single fault assumption [5]. The Advanced RAIM (ARAIM) technique [6] extends its monitoring ability to multiple faults assumption and multi-constellation GNSS observables. The above-mentioned RAIM/ARAIM approaches for open sky environments are not effective in ensuring integrity in degraded urban scenarios due to the unique circumstances such as limited satellite visibility, multipath and Non-line-of-sight (NLOS) effects, resulting in the difficulty to have a reliable uncertainty model of the received measurements [3]. In addition, the conventional GNSS IM tends to directly exclude the faulty GNSS measurements until the Chi-square test is passed given a pre-defined probability of risk, which can significantly degrade the satellite geometry in urban canyons. Besides, both RAIM/ARAIM consider all pseudorange measurements in one single epoch and provide a loose bound of integrity risk, which is suitable in aviation but it could be too conservative for vehicles in urban scenarios [7]. Recent advances in integrity monitoring for ground vehicles in urban canyons also extend its application to multi-modal sensors (e.g., inertial navigation system (INS), Radar, LiDAR, Camera) [8] and Kalman filtering [9, 10] to guarantee the safety redundancy. However, they still suffer from the high cost of INS sensors and face the lack of measurement redundancy brought by frequent and multiple multipath and NLOS receptions [3].

Our previous studies utilize Factor Graph Optimization (FGO) for GNSS positioning [11-14] which improved the measurement redundancy by considering all historical information and obtains better positioning accuracy compared to Kalman filtering with its ability to conduct multiple iterations and linearization [14]. By further applying FDE for all historical measurements, [15] conducts a Chi-square test over multiple epochs and shows that more redundant measurements result in better FDE performance. However, performance improvement is limited when most of measurements are faulty, or the given uncertainty modeling is not correct. On the other hand, the conventional

RAIM/ARAIM technique operates separately alongside the positioning part, meaning that the positioning results obtained from all measurements provide an initial guess for integrity monitoring, then fault measurements are excluded via FDE. After that, PL and new positioning results are obtained correspondingly. Such kind of separation is not robust in two aspects: 1) when healthy measurements are excluded, they cannot be reconsidered in the next iteration of integrity monitoring, and 2) when corresponding measurement variance is incorrect, FDE may fail, and the calculated PL cannot well-bound position error. *Can we automatically select/exclude fault measurements and estimate measurement uncertainty simultaneous to alleviate the challenges listed above?* In fact, the recently developed switch variable algorithm [16] is one good candidate.

The concept of switch variable (SV) was initially introduced in SLAM (Simultaneous Localization and Mapping) community to detect and remove outlier constraints from factor graph problems [16], later it has also been exploited in GNSS positioning to identify and remove multipath or NLOS affected measurements in urban canyons, without any additional a priori knowledge or additional sensor information [17]. The SV is implemented by associating switch variable with each pseudorange measurement factor that could potentially be an outlier. [18] also utilized switch variable for FGO-based GNSS positioning and won the first-place award of the Google smartphone decimeter challenge in both 2021 and 2022. Specifically, the switch variable is designed to continuously range from 0 to 1, where 0 indicates exclusion of the corresponding measurement and 1 denotes measurement selection as an inlier, whereas a value between 0 and 1 accounts for measurement variance modification [18]. It is therefore feasible to apply the switch variable to incorporate FDE into GNSS positioning by FGO: *The test statistics is represented as sum of normalized residuals of switch variable-associated pseudorange factors inside factor graph, and its threshold depends on the measurement amount and a given false alarm probability.* Hence, the inequality constraint arising from the Chi-square test in FDE can be formulated by ensuring that the chi-square test statistic is equal or less than the threshold. In such a way, the additional switch variables can be iteratively estimated to satisfy the chi-square test inequality constraint, meaning that all involved measurements are iteratively identified during optimization and therefore avoiding the exclusion of healthy measurements. Protection level (PL) can be either calculated or estimated accordingly following the idea of RAIM/ARAIM while considering the reweighting effect of switch variables.

In this study, switch variables will be applied on a conventional factor graph based GNSS positioning framework, as an attempt to demonstrate its potential to improve RAIM performance. In this paper, only pseudorange measurements are considered in batch FGO. First, FGO with switch variable together with the switch prior factors that aim to avoid local minimum will be implemented. Then, the above-mentioned FDE inequality constraint will be formulated analytically. Next, the PL will be calculated utilizing geometry matrix. The whole FGO framework will be evaluated in terms of performance of FDE constraint and PL compared to the conventional FGO-based positioning without switch variable [15].

The remainder of this paper is structured as follows: an overview of the proposed method is shown in Section II. The GNSS positioning using FGO with switch variables is introduced in Section III. Then, the experiments are conducted to analyze the performance of our proposed method in Section IV. Finally, we will present the conclusion and summarize the future work in Section V.

II. OVERVIEW OF THE PROPOSED METHOD

The flowchart of the proposed method is shown in Fig. 1. The inputs of the system are raw pseudorange measurements received by the GNSS receiver. The pseudorange measurement, satellite position and clock bias, as well as the *goGPS* weighting matrix based on C/N0 and the elevation angle [19] are fetched from the raw data. Then, by associating the pseudorange measurements with switch variables, the switchable factors are constructed. Besides, based on the concept of chi-square test in FDE, the chi-square test factor are constructed with the total pseudorange amount M , switchable pseudorange residual and the given false alarm rate P_{FA} . Moreover, the utilization of switch variables motivates two types of factors: switch prior factors and switch reliable factors. Later, after solving the factor graph formulated by the above-mentioned four types of factors, the state estimation as well as the geometry matrix are obtained. After that, the modified weighting matrix are obtained using the switch state estimations as well as the *goGPS* weighting matrix. Finally, the HPL is derived based on the modified weighting matrix, the geometry matrix and the test threshold T_D^* . Specifically, we employ the method of [5] to calculate HPL with the single-fault assumption, whereas the geometry matrix and T_D^* considers switchable pseudorange factors involved in a single epoch.

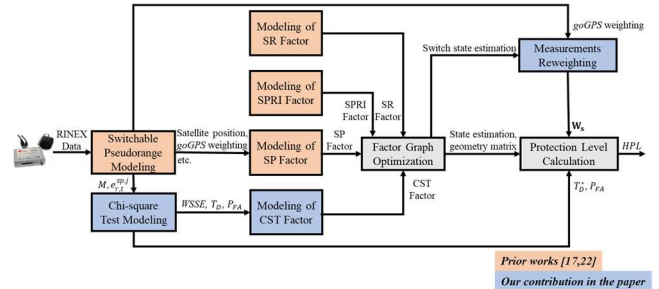


Fig. 1. Flowchart of our proposed method in this paper. The SR, SPRI, SP and CST denote switch reliable, switch prior, switch pseudorange and chi-square test factor, respectively. M represents the total measurements amount inside the graph, $e_{r,t}^{sp,j}$ stands for the switchable pseudorange residual, and W_s is the modified weighting matrix.

The contributions of this paper are summarized as follows:

- (1) This paper proposes to incorporate FDE into FGO through switch variables to improve measurement redundancy by dynamically reweighting the measurements through the switchable variable constraint.
- (2) This paper proposes a new approach for PL calculation that consider the reweighting effect of switch variables to bound the position error accurately, which is further validated using the dataset collected in Hong Kong.

III. METHODOLOGY

This section presents the methodology of the integrity-constrained FGO for GNSS positioning. In this paper, only pseudorange measurements from the global positioning system (GPS) and BeiDou are utilized to conduct integrity monitoring. The states of the GNSS receiver are represented as follows:

$$\boldsymbol{\chi} = [\mathbf{x}_{r,1}, \mathbf{x}_{r,2}, \dots, \mathbf{x}_{r,n}] \quad (1)$$

where $\boldsymbol{\chi}$ denotes the set of states of the GNSS receiver r from the first epoch to the current epoch n . The state of the GNSS receiver r at a single epoch t can be expressed as follows:

$$\mathbf{x}_{r,t} = (\mathbf{p}_{r,t}, \boldsymbol{\delta}_{r,t}, s_{r,t}^1, s_{r,t}^2, \dots, s_{r,t}^m)^T \quad (2)$$

where $t \in (1, n)$, the state $\mathbf{x}_{r,t}$ includes the position $\mathbf{p}_{r,t} (p_{r,t,x}, p_{r,t,y}, p_{r,t,z})$ in the ECEF coordinate, the receiver clock bias $\boldsymbol{\delta}_{r,t} (\delta_{r,t}^{GPS}, \delta_{r,t}^{BDS})$ of both GPS and BeiDou. $s_{r,t}^j$ denotes the switch variable associated with the satellite. Specifically, each switch variable $s_{r,t}^j$ ranges between 0 to 1, where 0 denotes measurement exclusion and 1 for measurement selection, whereas a switch value between 0 and 1 represents measurement reweighting [18]. The initial switch value is set to 1. The superscript j denotes the index of the satellites, and m is the total amount of received satellites at epoch t .

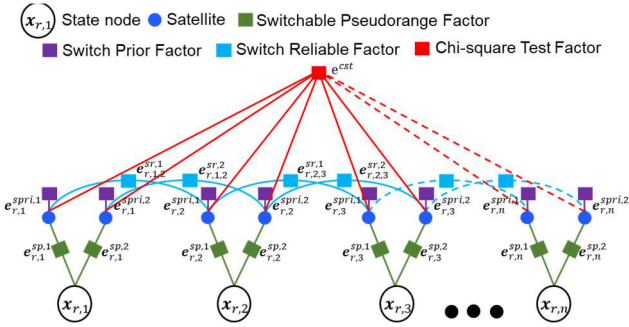


Fig. 2. Graph structure of the proposed integrity-constrained factor graph. The blue circle denotes the satellite. Only two satellites are drawn at each epoch for simplicity. The green shaded rectangle represents the switchable pseudorange factor (e.g., $e_{r,t}^{sp,j}$). The purple shaded rectangle denotes the switch prior factor (e.g., $e_{r,t}^{spri,j}$). The light blue rectangle stands for the switch reliable factor (e.g., $e_{r,t,t+1}^{sr,j}$). The red rectangle denotes the chi-square test factor (e.g., e^{cst}). The white circle represents the state of the GNSS receiver.

The graph structure of the proposed integrity-constrained factor graph optimization is illustrated in Fig. 2. The subscript n of state node is the total measurement epochs involved in the FGO. If the same satellite j appears in consecutive states, then the switch variable associated with the satellite j will be connected using the switch reliable factor. The chi-square-test factor is connected with all switch variables in the FGO. Specifically, our proposed method utilizes the chi-square test factor to conduct a batch form FDE by considering all pseudorange measurements among epochs. The calculation of horizontal protection level is based on the single fault assumption [5] while considering the reweighting effect of switch variables.

A. Switchable Pseudorange Factor

Each raw pseudorange measurement $\rho_{r,t}^j$ from satellite j are obtained by the GNSS receiver, which is denoted as follows:

$$\rho_{r,t}^j = r_{r,t}^j + c(\delta_{r,t} - \delta_{r,t}^j) + I_{r,t}^j + T_{r,t}^j + \varepsilon_{r,t}^j \quad (3)$$

where $r_{r,t}^j$ is the geometric range between the satellite j and the GNSS receiver r at epoch t . c denotes the speed of the light. For simplicity, $\delta_{r,t}$ represents the receiver clock bias from single satellite constellation (GPS or BeiDou). $\Delta_{r,t}^j$ indicates the clock bias of satellite. $I_{r,t}^j$ and $T_{r,t}^j$ represent the ionospheric and the tropospheric delay error, respectively, and they are modeled following the method in RTKLIB [20]. Besides, $\varepsilon_{r,t}^j$ represents the errors introduced by multipath and NLOS receptions, receiver noise and antenna phase-related noise.

The observation model for GNSS pseudorange measurement from a given satellite j is illustrated as follows:

$$\rho_{r,t}^j = h_{r,t}^j(\mathbf{p}_{r,t}, \mathbf{p}_t^j, \delta_{r,t}) + \omega_{r,t}^j \quad (4)$$

$$\text{with } h_{r,t}^j(\mathbf{p}_{r,t}, \mathbf{p}_t^j, \delta_{r,t}) = \|\mathbf{p}_t^j - \mathbf{p}_{r,t}\| + \delta_{r,t}$$

where $\mathbf{p}_{r,t}$ and \mathbf{p}_t^j denote the position of the receiver and the position of the satellite at epoch t , respectively. The term $\omega_{r,t}^j$ represents the Gaussian white noise with $\omega_{r,t}^j \sim \mathcal{N}(0, \Sigma_{r,t}^j)$. Here $\Sigma_{r,t}^j$ denotes the covariance of the satellite j , which is calculated based on SNR and the satellite elevation angle [19]. Therefore, the error function $e_{r,t}^{sp,j}$ of switchable pseudorange factor for a given measurement $\rho_{r,t}^j$ is derived as follows:

$$\|e_{r,t}^{sp,j}\|_{\Sigma_{r,t}^j}^2 = \|s_{r,t}^j \cdot e_{r,t}^{sp,j}\|_{\Sigma_{r,t}^j}^2 \quad (5)$$

$$\text{with } e_{r,t}^{sp,j} = \rho_{r,t}^j - h_{r,t}^j(\mathbf{p}_{r,t}, \mathbf{p}_t^j, \delta_{r,t})$$

where $s_{r,t}^j$ represents the switch variable associated with satellite j , and $e_{r,t}^{sp,j}$ denotes the corresponding pseudorange residual.

B. Switch Prior Factor

Initially all satellites are accepted as healthy satellites, the switch prior factor is therefore used to anchor the switch variables at the initial value of 1. Besides, the utilization of switch prior factors also prevents the optimization process from getting stuck into local minimum with all zero switch values [17, 18]. The corresponding error function $e_{r,t}^{spri,j}$ is given as follows:

$$\|e_{r,t}^{spri,j}\|_{\Sigma_{r,t}^{spri,j}}^2 = \|s_{r,t}^j - 1\|_{\Sigma_{r,t}^{spri,j}}^2 \quad (6)$$

where $\Sigma_{r,t}^{spri,j} = 1$ is the covariance of the switch prior factor.

C. Switch Reliable Factor

Since pseudorange measurements from the same satellite are time-correlated among epochs, the switch variable from the same satellite in consecutive epochs is likely to be equal [21]. The switch reliable factor here acts as a constraint to avoid the switch variable changing rapidly [22], which leads to the following error function formulation:

$$\|e_{r,t,t+1}^{sr,j}\|_{\Sigma_{r,t,t+1}^{sr,j}}^2 = \|s_{r,t}^j - s_{r,t+1}^j\|_{\Sigma_{r,t,t+1}^{sr,j}}^2 \quad (7)$$

where $\Sigma_{r,t,t+1}^{sr,j} = 1$ is the covariance of the switch reliable factor.

D. Chi-square Test Factor

The conventional Chi-square test in RAIM [5] considers all pseudorange measurements in single epoch, the Chi-square test factor, however, involves all pseudorange measurements in the graph. The detailed formulation is described as follows:

First, the m switchable pseudorange residuals at the epoch t is denoted as:

$$\mathbf{e}_{r,t}^{sp} = (e_{r,t}^{sp,1}, \dots, e_{r,t}^{sp,m})^T \quad (8)$$

then, the normalized residuals can be formulated as:

$$\mathbf{e}_{r,t} = (e_{r,t}^{sp,1}/\sigma_{r,t}^1, \dots, e_{r,t}^{sp,m}/\sigma_{r,t}^m)^T \quad (9)$$

$$\text{with } \sigma_{r,t}^j = \sqrt{\Sigma_{r,t}^j}$$

where $\sigma_{r,t}^j$ is the standard deviation of the pseudorange measurement j . Considering that there are totally n epochs inside the graph, the normalized residuals among n epochs is represented as:

$$\mathbf{e}_m = (\mathbf{e}_{r,1}, \dots, \mathbf{e}_{r,m})^T \quad (10)$$

therefore, the test statistics can be formulated as the Weighted Sum of the Squared Errors ($WSSE$) over all switchable pseudorange residuals among epochs:

$$WSSE = \mathbf{e}_m^T \mathbf{e}_m \quad (11)$$

Specifically, we assume that there are totally M pseudorange measurements observed in the graph. Then, a comparison of \sqrt{WSSE} with threshold $T_D(v, P_{FA})$, which is based on the degree of freedom of the chi-square distribution $v = M - 5n$, and the pre-defined false alarm rate P_{FA} , is conducted. If \sqrt{WSSE} is below the threshold $T_D(v, P_{FA})$, then the position estimation is assumed to be safe with a false alarm rate P_{FA} . Therefore, the error function e^{cst} of the chi-square test factor can be formulated as follows:

$$\|e^{cst}\|_{\Sigma^{cst}}^2 = \|\alpha(\sqrt{WSSE} - T_D)\|_{\Sigma^{cst}}^2 \quad (12)$$

$$\text{with } \alpha = 1, \Sigma^{cst} = 1$$

where α is the step size parameter, and Σ^{cst} denotes the covariance of the corresponding residual.

E. GNSS Positioning via FGO

Based on the factors derived above, the objective function for GNSS positioning via FGO is formulated as follows:

$$\begin{aligned} \mathbf{x}^* = \arg \min_{\mathbf{x}} & \sum_{j,t} \|e_{r,t}^{sp,j}\|_{\Sigma_j}^2 + \|e_{r,t}^{spri,j}\|_{\Sigma_{spri,j}}^2 + \\ & \|e_{r,t,t+1}^{sr,j}\|_{\Sigma_{sr,j}}^2 + \|e^{cst}\|_{\Sigma^{cst}}^2 \end{aligned} \quad (13)$$

the variable \mathbf{x}^* stands for the optimal state sets estimation, which is obtained by solving the objective function (13). In this paper, Ceres [23] is utilized as the nonlinear optimization solver.

In order to prevent the optimization problem from rejecting all measurements with all zero switch values, the following initialization strategy is adopted when the new epoch $t + 1$ comes:

- (1) The previous estimation results $\hat{\mathbf{x}}_{r,1}, \dots, \hat{\mathbf{x}}_{r,t}$ is assigned as initial guesses for the previous states $\mathbf{x}_{r,1}, \dots, \mathbf{x}_{r,t}$.
- (2) If the satellite j is observed at both epoch t and $t + 1$, then $\hat{\mathbf{x}}_{r,t}^j$ serves as the initial guess for the state $s_{r,t+1}^j$, otherwise 1 is assigned as the initial guess.
- (3) If the satellite amount at epoch $t + 1$ is larger than 4, then the corresponding single point positioning result serves as the initial guess of $\mathbf{p}_{r,t+1}$ and $\delta_{r,t+1}$; otherwise the initial guess is provided by last estimation results $\hat{\mathbf{p}}_{r,t}$ and $\hat{\delta}_{r,t}$.

F. Protection Level Calculation

According to [24, 25], the effect of switch variables over covariance can be interpreted as follows:

$$\mathbf{W}_s = \text{diag}(s_{r,t}^1, s_{r,t}^2, \dots, s_{r,t}^m)^2 \mathbf{W} \quad (14)$$

$$\text{with } \mathbf{W} = \text{diag}(\Sigma_{r,t}^1, \Sigma_{r,t}^2, \dots, \Sigma_{r,t}^m)^{-1}$$

where the weighting matrix \mathbf{W} denotes the inverse of covariance matrix of obtained m pseudorange measurements in epoch t , and \mathbf{W}_s stands for the modified weighting matrix. Next, let $\mathbf{y}_{r,t}^p = (e_{r,t}^{p,1}, e_{r,t}^{p,2}, \dots, e_{r,t}^{p,m})^T$ denotes the vector containing m pseudorange residuals in single epoch, and $\Delta \mathbf{x}_t^p = (\Delta p_{r,t,east}, \Delta p_{r,t,north}, \Delta p_{r,t,up}, \Delta \delta_{r,t})^T$ represents the five dimensional offsets vector (east, north, up, GPS clock and BeiDou clock) near a fixed linearization point from the last iteration. The linearized pseudorange observation model in single epoch is formulated as:

$$\mathbf{y}_{r,t}^p = \mathbf{G} \Delta \mathbf{x}_t^p + \boldsymbol{\varepsilon} \quad (15)$$

where \mathbf{G} is the geometry matrix with the dimension $m \times 5$, and $\boldsymbol{\varepsilon}$ is the ranging errors with the covariance matrix \mathbf{W}_s^{-1} . Then, the weighted least square estimate of $\Delta \mathbf{x}_t^p$ can be written as:

$$\Delta \hat{\mathbf{x}}_t^p = \mathbf{A} \mathbf{y}_{r,t}^p \quad (16)$$

where:

$$\mathbf{A} = (\mathbf{G}^T \mathbf{W}_s \mathbf{G})^{-1} \mathbf{G}^T \mathbf{W}_s \quad (17)$$

the estimate of the ranging errors is:

$$\hat{\boldsymbol{\varepsilon}} = \mathbf{y}_{r,t}^p - \mathbf{G} \Delta \hat{\mathbf{x}}_t^p = (\mathbf{I} - \mathbf{G} \mathbf{A}) \mathbf{y}_{r,t}^p \quad (18)$$

from the error estimates we can calculate $WSSE$ in single epoch [5, 26]:

$$\begin{aligned} WSSE^* &= \hat{\boldsymbol{\varepsilon}}^T \mathbf{W}_s \hat{\boldsymbol{\varepsilon}} \\ &= [(\mathbf{I} - \mathbf{G} \mathbf{A}) \mathbf{y}_{r,t}^p]^T \mathbf{W}_s [(\mathbf{I} - \mathbf{G} \mathbf{A}) \mathbf{y}_{r,t}^p] \end{aligned} \quad (19)$$

which can be simplified to [5]:

$$WSSE^* = \mathbf{y}_{r,t}^{p\ T} \mathbf{S} \mathbf{y}_{r,t}^p \quad (20)$$

with

$$\mathbf{S} = \mathbf{W}_s (\mathbf{I} - \mathbf{G} \mathbf{A}) \quad (21)$$

If the batch version of chi-square test in section D is passed, which means $\sqrt{WSSE} \leq T_D(v, P_{FA})$, then the following inequality also holds:

$$WSSE^* \leq T_D^*(v^*, P_{FA}) \quad (22)$$

where $T_D^*(v^*, P_{FA})$ is the test statistics threshold considering the pseudorange measurement amount m at epoch t , and the degree of freedom of chi-square distribution is $v^* = m - 5$. After passing the chi-square test described in section D, the method proposed in [5, 26] protects for bias and noise under single fault assumption with the horizontal protection level derived as follows:

$$HPL = \max \left\{ \sqrt{\frac{A_{1,i}^2 + A_{2,i}^2}{S_{ii}}}; i = 1, \dots, m \right\} T_D^* + k_H HRMS \quad (23)$$

where:

$$HRMS = \sqrt{(\mathbf{G}^T \mathbf{W}_s \mathbf{G})_{1,1}^{-1} + (\mathbf{G}^T \mathbf{W}_s \mathbf{G})_{2,2}^{-1}} \quad (24)$$

here k_H denotes the number of the standard deviation, which is empirically set to 3 based on the 3σ rule. Due to the page's limitations, we refer the readers to [5, 26] for more details of protection level calculation under single fault assumption.

IV. EXPERIMENT RESULTS AND DISCUSSIONS

To assess the performance of the proposed method in this paper, the proposed method is evaluated using real pseudorange observables in open sky scenario. The receiver is static and P_{FA} is set to 10^{-4} during the whole experiments. During the experiment, the raw GPS/BeiDou measurements are collected by a u-blox M8T GNSS receiver at a frequency of 1Hz, totally 16 satellites are observed. Additionally, we inject gaussian random errors to observables from satellites of PRN 2, 6, 15 with a mean $\mu = 15$ m and a standard deviation $\sigma = 5$ m to introduce faulty measurements. For simplicity, we regard the measurements with injected biases as the faulty measurements and ignore the potential faults in remaining satellites. The ground truth location represented in latitude, longitude, and altitude is: $[114.17^\circ, 22.31^\circ, 63 \text{ m}]$.

The experiments are implemented in a desktop computer with an Intel Core i9-12900K CPU. In order to evaluate the contribution of this paper, the following methods are compared:

- (1) **FGO**: GNSS positioning using only pseudorange measurements, which is equivalent to the single point positioning (SPP).
- (2) **RAIM-FGO**: GNSS positioning using only pseudorange measurements in FGO. Meanwhile, the faulty measurements are manually excluded at each epoch to simulate the snapshot FDE.
- (3) **SW-FGO**: Switchable pseudorange factors, along with switch prior factors and switch reliable factors are incorporated into the FGO for GNSS positioning.
- (4) **SWFDE-FGO (proposed method)**: All four kinds of factors illustrated in Fig. 2 are used inside the FGO for GNSS positioning. Compared to RAIM-FGO, the proposed method conducts a batch FDE with the help of the chi-square test factor.

The positioning performance is evaluated in the east, north, and up (ENU) frames. Since we are conducting the

GNSS positioning for ground vehicle, only the horizontal positioning and integrity performance are evaluated.

A. Evaluation on Positioning Accuracy and HPL

The error and HPL of GNSS positioning using the four above-mentioned methods is shown in TABLE I. The mean error of 3.23 meters is achieved using only pseudorange factors in FGO, with a smallest mean HPL of 11.70 meters. By applying snapshot-FDE in FGO, RAIM-FGO manually excluded the faulty measurements, resulting a lower mean 2d error of 2.72 meters, with a slightly increased mean HPL of 13.11 meters. Interestingly, both SW-FGO and SWFDE-FGO achieves better positioning accuracy but larger HPL than the first two methods, which shows that switch variables can reweight the measurements and hence influence the positioning performance. Specifically, SWFDE-FGO obtains the lowest 2D error of 1.31 meters and a less conservative HPL compared to SW-FGO. The bound rate of HPL is defined as the percentage of $HPL \geq \text{error}$. The GNSS IM is satisfied if the calculated HPL can bound the actual 2D error. The bound rates are 100% for four methods, which indicates that the *goGPS* weighting [19] for this open-sky scenario is conservative.

TABLE I. GNSS POSITIONING PERFORMANCE

Items	FGO	RAIM-FGO	SW-FGO	SWFDE-FGO
Mean 2D error (m)	3.23	2.72	1.78	1.31
Mean HPL (m)	11.70	13.11	26.24	20.30
Bound Rate (%)	100	100	100	100

B. Evaluation on Chi-square Test Factor

Fig. 3 illustrates the errors (solid curve) and HPLs (dashed curve) during the experiments, and the shaded gray area denotes the biases injection period. During the biases injection period, SW-FGO (green) and SWFDE-FGO (pink) are below the error of FGO (blue), which indicate that both switch variables itself and switch variables plus chi-square-test factors act as FDE to ease the effect of faulty measurements.

To further show the effectiveness of integrity monitoring using the proposed method, the skyplot of the 4 methods at epoch A are given in the Fig. 4. Note that the circle size represents switch values, and switch values are assigned as 1 for FGO and RAIM-FGO. Compared to RAIM-FGO, which holds the *goGPS* weighting [19] and conducts FDE by simply exclude the faulty measurements, both SW-FGO and SWFDE-FGO conducts FDE by assigning small switch values to the faulty measurements. Such kind of FDE maintains the geometry and obtains an optimal weighting during the positioning. Notice that even a healthy satellite can still obtain a small switch value (e.g., PRN 52), the main reason is that the measurements still suffer from the ionospheric and the tropospheric delay error without double-differencing technique. Besides, SWFDE-FGO tends to assign larger switch values than SW-FGO (e.g., PRN 15, 19 and 62), since larger switch values keep $WSSE$ closer to T_D^2 , hence reduce the error of chi-square test factor e^{cst} .

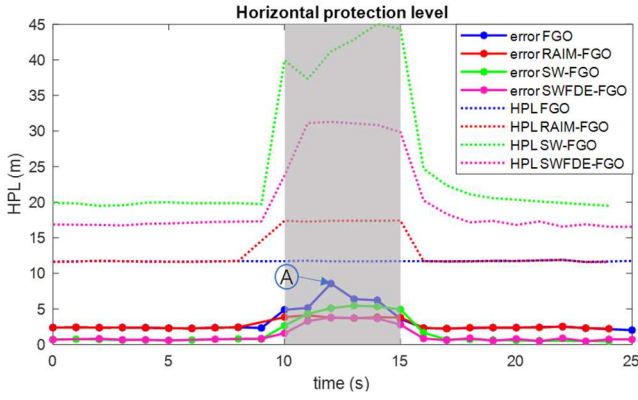


Fig. 3. The error (solid line) and HPL (dashed line) of four listed methods: FGO (blue), RAIM-FGO (red), SW-FGO (green), SWFDE-FGO (pink). During the gray shaded area between 10s and 15s, the random biases are injected on the satellite of PRN 2, 6, and 15.

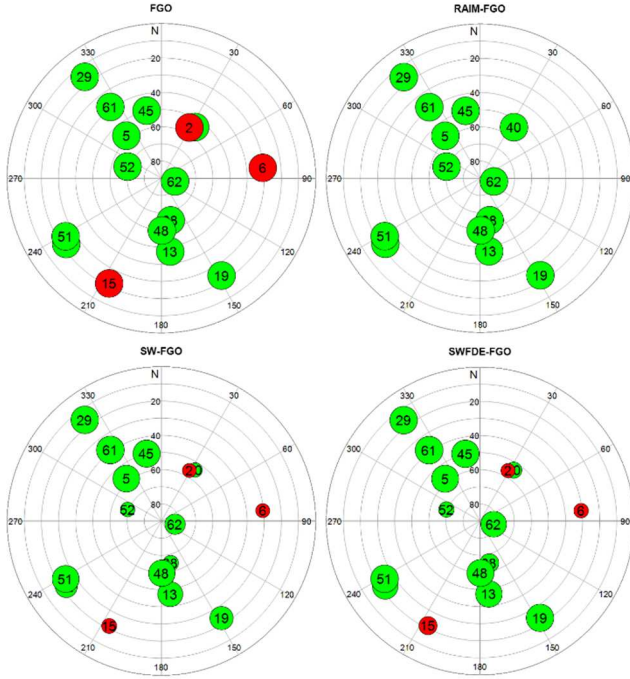


Fig. 4. The skyplot of the four methods at epoch "A". The red shaded circle denotes the faulty measurements with random injected biases, and the green circle denotes the healthy satellites. The circle size represents switch values, each circle is assigned with the corresponding PRN number. Note that for FGO and RAIM-FGO, switch values are assigned as 1.

C. Evaluation on HPL Calculation

It can be observed from the Table 1 that SWFDE-FGO achieves less conservative HPL than SW-FGO, the main reason lies in the different switch values estimation of both methods. More details will be given in this part.

Fig. 5 shows the squared $WSSE$ of single epoch ($\sqrt{WSSE^*}$) during the experiments, the black dashed curve denotes the initial test statistic threshold $T_D^*(v^*, P_{FA})$ with $v^* = 16 - 5$ and $P_{FA} = 10^{-4}$. FGO has the largest $\sqrt{WSSE^*}$ due to the faulty measurements, RAIM-FGO (red curve) stays close to T_D^* because it excludes the faulty measurements but keeps the original conservative weighting matrix. Due to the potential faults except PRN 2, 6 and 15, the statistic of RAIM-FGO always exceeds the threshold. It is anticipated that the fault-free statistic will stay below the threshold value if the experiment is conducted using simulated open sky

data. SW-FGO and SWFDE-FGO both obtain $\sqrt{WSSE^*}$ lower than T_D^* since it reweights all measurements inside the geometry. The chi-square test factors can keep $\sqrt{WSSE^*}$ closer to T_D^* , which leads to a relative larger switch variables estimation.

Fig. 6 illustrates the relationship between the absolute pseudorange residuals ($\|e_{r,t}^{p,j}\|$) and the switch variables ($s_{r,t}^j$). It is confirmed that for a value of absolute pseudorange residual, SWFDE-FGO estimate a larger switch value compared SW-FGO, let $\mathbf{W}_{s,SWFDE}$, HPL_{SWFDE} and $\mathbf{W}_{s,SW}$, HPL_{SW} denote the modified weighting matrix and HPL of SWFDE-FGO and SW-FGO, respectively. We have:

$$\mathbf{W}_{s,SWFDE} \geq \mathbf{W}_{s,SW} \quad (25)$$

based on the equation. (17), (21) and (23) we can therefore conclude that $\text{HPL}_{SWFDE} \leq \text{HPL}_{SW}$. The main reason for this phenomenon is that: switch variables behave aggressively in assigning the switch values to measurements with the relatively larger absolute pseudorange residual, while these measurements may still benefit the positioning. With the help of FDE concept introduced from the integrity monitoring knowledge, the chi-square test factor can provide more suitable switch values that promise lower positioning error and less-conservative HPL.

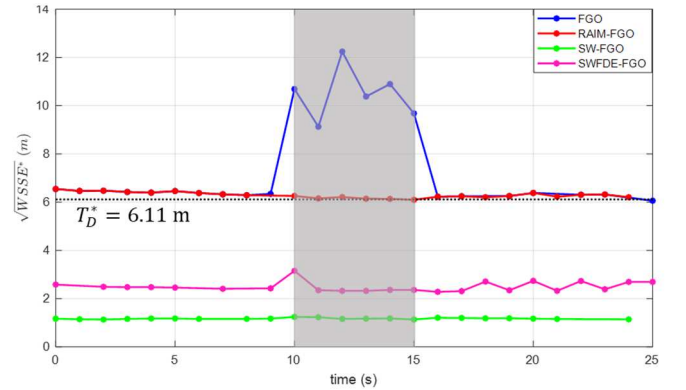


Fig. 5. The squared $WSSE$ of single epoch ($\sqrt{WSSE^*}$) of each method compared with test statistic threshold T_D^* (black dashed curve). The gray shaded area denotes the bias injection period.

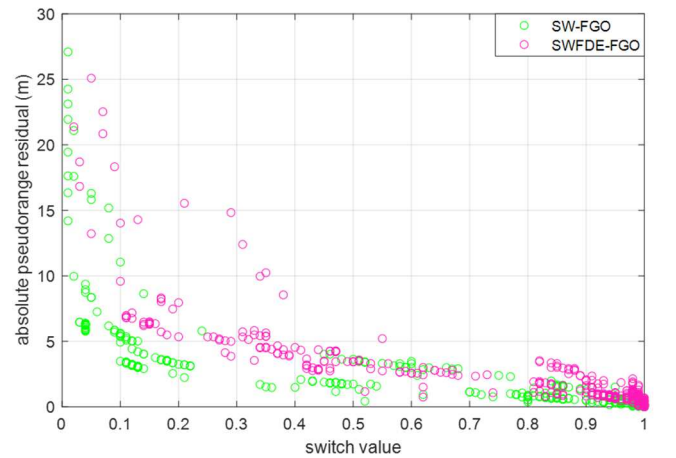


Fig. 6. Relationship between switch values ($s_{r,t}^j$) and absolute pseudorange residuals ($\|e_{r,t}^{p,j}\|$) for all measurements during the experiment. The green dots denote SW-FGO while pink dots stand for SWFDE-FGO.

V. CONCLUSION AND FUTURE WORK

This paper proposed a new framework of RAIM for graph-based GNSS positioning, including both FDE and PL calculation. Firstly, an integrity-constrained factor graph optimization for GNSS positioning is proposed, where the FDE concept in conventional RAIM is combined with positioning by incorporating the chi-square test factor into the factor graph. Then, the HPL is calculated separately considering the reweighting effect of switch variables.

We evaluate the proposed framework in the open-sky scenario with manually injected biases. It is shown that the proposed method can effectively conduct FDE by reweighting the measurements while maintaining the geometry. Moreover, we also show that the calculated HPL can well bound the position error. However, the HPL calculation, which operates alongside the positioning, is still conservative under single fault assumption. In the future, we will consider incorporating HPL calculation into factor graph, in the hope of providing tighter value. Besides, we will also verify the proposed method using more real data in challenging urban environments. Moreover, in order to provide correct weighting for pseudorange measurements, we will evaluate the proposed method using Differential GNSS technique.

ACKNOWLEDGMENT

This research is financially supported by the Research Impact Fund Scheme under Hong Kong University Grants Committee. The project title is "Resilient Urban PNT Infrastructure to Support Safety of UAV Remote Sensing in Urban Regions". The authors would like to thank Yihan Zhong, Hoi-Fung Ng and Liyuan Zhang for their support with the dataset preparation.

REFERENCES

- [1] Y. J. Morton, F. van Diggelen, J. J. Spilker Jr, B. W. Parkinson, S. Lo, and G. Gao, *Position, navigation, and timing technologies in the 21st century: Integrated satellite navigation, sensor systems, and civil applications, volume 1*. John Wiley & Sons, 2021.
- [2] P. Zabalegui, G. De Miguel, A. Pérez, J. Mendizabal, J. Goya, and I. Adin, "A review of the evolution of the integrity methods applied in GNSS," *IEEE Access*, vol. 8, pp. 45813-45824, 2020.
- [3] N. Zhu, J. Marais, D. Bétaille, and M. Berbineau, "GNSS position integrity in urban environments: A review of literature," *IEEE Transactions on Intelligent Transportation Systems*, vol. 19, no. 9, pp. 2762-2778, 2018.
- [4] R. G. Brown, "A baseline GPS RAIM scheme and a note on the equivalence of three RAIM methods," *Navigation*, vol. 39, no. 3, pp. 301-316, 1992.
- [5] T. Walter and P. Enge, "Weighted RAIM for precision approach," in *PROCEEDINGS OF ION GPS*, 1995, vol. 8, no. 1: Institute of Navigation, pp. 1995-2004.
- [6] J. Blanch *et al.*, "Advanced RAIM user algorithm description: Integrity support message processing, fault detection, exclusion, and protection level calculation," in *Proceedings of the 25th International Technical Meeting of The Satellite Division of the Institute of Navigation (ION GNSS 2012)*, 2012, pp. 2828-2849.
- [7] S. Pullen, T. Walter, and P. Enge, "SBAS and GBAS integrity for non-aviation users: moving away from" specific risk", in *Proceedings of the 2011 International Technical Meeting of The Institute of Navigation*, 2011, pp. 533-545.
- [8] Q. Meng and L.-T. Hsu, "Integrity monitoring for all-source navigation enhanced by Kalman filter-based solution separation," *IEEE Sensors Journal*, vol. 21, no. 14, pp. 15469-15484, 2020.
- [9] S. Bhattacharyya and D. Gebre-Egziabher, "Kalman filter-based RAIM for GNSS receivers," *IEEE Transactions on Aerospace and Electronic Systems*, vol. 51, no. 3, pp. 2444-2459, 2015.
- [10] M. Joerger and B. Pervan, "Integrity risk of Kalman filter-based RAIM," in *Proceedings of the 24th International Technical Meeting of The Satellite Division of the Institute of Navigation (ION GNSS 2011)*, 2011, pp. 3856-3867.
- [11] X. Bai, W. Wen, and L.-T. Hsu, "Time-correlated Window Carrier-phase Aided GNSS Positioning Using Factor Graph Optimization for Urban Positioning," *IEEE Transactions on Aerospace and Electronic Systems*, 2022.
- [12] S. Das, R. Watson, and J. Gross, "Review of Factor Graphs for Robust GNSS Applications," *arXiv preprint arXiv:2112.07794*, 2021.
- [13] W. Wen and L.-T. Hsu, "Towards robust GNSS positioning and Real-time kinematic using factor graph optimization," in *2021 IEEE International Conference on Robotics and Automation (ICRA)*, 2021: IEEE, pp. 5884-5890.
- [14] W. Wen, T. Pfeifer, X. Bai, and L.-T. Hsu, "Factor graph optimization for GNSS/INS integration: A comparison with the extended Kalman filter," *NAVIGATION: Journal of the Institute of Navigation*, vol. 68, no. 2, pp. 315-331, 2021.
- [15] W. Wen, Q. Meng, and L.-T. Hsu, "Integrity monitoring for GNSS positioning via factor graph optimization in urban canyons," in *Proceedings of the 34th International Technical Meeting of the Satellite Division of The Institute of Navigation (ION GNSS+ 2021)*, 2021, pp. 1508-1515.
- [16] N. Sünderhauf and P. Protzel, "Switchable constraints for robust pose graph SLAM," in *2012 IEEE/RSJ International Conference on Intelligent Robots and Systems*, 2012: IEEE, pp. 1879-1884.
- [17] N. Sünderhauf, M. Obst, S. Lange, G. Wanielik, and P. Protzel, "Switchable constraints and incremental smoothing for online mitigation of non-line-of-sight and multipath effects," in *2013 IEEE Intelligent Vehicles Symposium (IV)*, 2013: IEEE, pp. 262-268.
- [18] T. Suzuki, "First place award winner of the smartphone decimeter challenge: global optimization of position and velocity by factor graph optimization," in *Proceedings of the 34th International Technical Meeting of the Satellite Division of The Institute of Navigation (ION GNSS+ 2021)*, 2021, pp. 2974-2985.
- [19] A. M. Herrera, H. F. Suhandri, E. Realini, M. Reguzzoni, and M. de Lacy, "goGPS: open-source MATLAB software," *GPS solutions*, vol. 20, no. 3, pp. 595-603, 2016.
- [20] T. Takasu and A. Yasuda, "Development of the low-cost RTK-GPS receiver with an open source program package RTKLIB," in *International symposium on GPS/GNSS*, 2009, vol. 1: International Convention Center Jeju Korea.
- [21] N. Sünderhauf, M. Obst, G. Wanielik, and P. Protzel, "Multipath mitigation in GNSS-based localization using robust optimization," in *2012 IEEE Intelligent Vehicles Symposium*, 2012: IEEE, pp. 784-789.
- [22] W. Li, X. Cui, and M. Lu, "A robust graph optimization realization of tightly coupled GNSS/INS integrated navigation system for urban vehicles," *Tsinghua Science and Technology*, vol. 23, no. 6, pp. 724-732, 2018.
- [23] S. Agarwal and K. Mierle, "Ceres solver: Tutorial & reference," *Google Inc*, vol. 2, no. 72, p. 8, 2012.
- [24] N. Sünderhauf, "Robust optimization for simultaneous localization and mapping," *Technischen Universität Chemnitz*, 2012.
- [25] N. Sünderhauf and P. Protzel, "Towards a robust back-end for pose graph slam," in *2012 IEEE international conference on robotics and automation*, 2012: IEEE, pp. 1254-1261.
- [26] J. E. Angus, "RAIM with multiple faults," *Navigation*, vol. 53, no. 4, pp. 249-257, 2006.